Spring 2016

Galvanically Induced/Accelerated Crevice Corrosion

Zachary R. Roland
zrr1@zips.uakron.edu

GALVANICALLY INDUCED/ACCELERATED CREVICE CORROSION

A Thesis

Presented to

The Graduate Faculty of The University of Akron

In Partial Fulfillment

of the Requirements for the Degree

Master of Science

Zachary R Roland

May, 2016

GALVANICALLY INDUCED/ACCELERATED CREVICE CORROSION

Zachary R Roland

Thesis

Approved:

Advisor
Dr. Curtis Clemons

Faculty Reader
Dr. Gerald Young

Faculty Reader
Dr. Kevin Kreider

Department Chair
Dr. Timothy Norfolk

Accepted:

Dean of the College
Dr. John Green

Dean of the Graduate School
Dr. Chand Midha

Date

ABSTRACT

In this thesis, a one dimensional model is developed to investigate the initial stages of corrosion in a fastener assembly consisting of a stainless steel fastener and aluminum 7075 as the plate. Differential equations are formulated and solved to determine the profiles for the potential, the oxygen concentration, and the aluminum ion concentration in the crevice, and also the potential in the bulk electrolyte. This fastener system exhibits galvanic corrosion, pitting corrosion, and crevice corrosion. It is found that the potential decreases monotonically down the length of the crevice, the oxygen concentration decreases exponentially down the length of the crevice, and the aluminum ion concentration builds up away from the mouth of the crevice. It is conjectured that the location of maximum aluminum ion concentration is where the most severe corrosion will occur. A parameter study is also done to study the effect of changes to the diffusivity, crevice width, and other parameters on the model calculations.

First off, I would like to thank Dr. Young, Dr. Kreider, and Dr. Clemons for all of their hard work. When time became a vital factor, they worked hard to make sure my work was not delayed. They were also vital in my understanding of the science behind my thesis. Without them, I would not have learned nearly as much as I have.

I would also like to thank my parents, Jennifer and Gregory Casey, as well as my sister, Alex Roland, for their support while writing this thesis. They gave me the space I needed when I needed it and supported me through the hardest times.

My friends, Alex Colwell, Kathryn Stalker, Eliza Jacops, and Matt Hughes, were very helpful. They provided a lot of technical assistance and emotional support as well that I needed to complete this thesis.

TABLE OF CONTENTS

LIST OF TABLES

LIST OF FIGURES

CHAPTER I

INTRODUCTION

Corrosion is of major concern when considering the structural integrity of systems composed of metals. It can cause heavy damage over time and result in the failure of metallic systems. It is important for manufacturing and maintenance purposes to be able to prevent, inhibit, or at the very least, predict corrosion so precautionary measures can be taken in an attempt to keep individuals involved in the use of said systems safe and allow prolonged use of the system. The system considered in this thesis is a fastener assembly commonly used in aircraft in the U.S. Air Force. The fasteners are composed of stainless steel, and the plates are composed of the aluminum alloy AA7075. Our goal is ultimately to be able to predict the damage due to corrosion in the crevice formed between the steel fastener and the aluminum plate. However, in this thesis, we only consider early time so we can study the mechanisms responsible for the initiation of corrosion, in turn allowing us to set up future investigation to further predict the damage. In order to understand the relevance of the problems solved here, it is ideal to first have a thorough understanding of corrosion mechanisms. The mechanisms we take into account are pitting corrosion, galvanic corrosion, and crevice corrosion.

Corrosion degradation of a metal can be due to a variety of mechanisms.

In all cases, there are four elements required in the system for corrosion to occur: an anode, a cathode, an electric pathway connecting the two (usually a metallic pathway), and an electrolyte. This setup is illustrated in Figure 1.1 using a galvanic cell. The anode is the negatively charged electrode, and the cathode is the positively charged electrode. The anode and cathode in this thesis are different metals, but different parts of the same metal can also act as the cathode or anode due to the chemistry in the system, as seen in [4]. Electrochemical reactions take place in the cell and on the surface of the metals causing electrons to travel from the anode to the cathode via the electric pathway. Anions created from the loss of electrons in the anode are expelled into the bulk electrolyte. Ions are atoms that have either gained or lost electrons, resulting in the atom to be positively charged (cations) or negatively charged (anions). An electron acceptor, or oxidizing agent, is required for this electron consumption to occur. This oxidizing agent is usually oxygen, and the depletion of oxygen becomes an area of concern when dealing with crevice corrosion.

The electrolyte plays an important part in the corrosion process. An electrolyte is a solution, or mixture, of ions in water. In our system, we assume there is a thin, electrolyte layer that naturally forms on the surface of the metals and in the crevice. The conductivity of the electrolyte describes how easy it is for ions to transport within the electrolyte. A larger conductivity corresponds to ions passing through the electrolyte more easily, and vice versa.

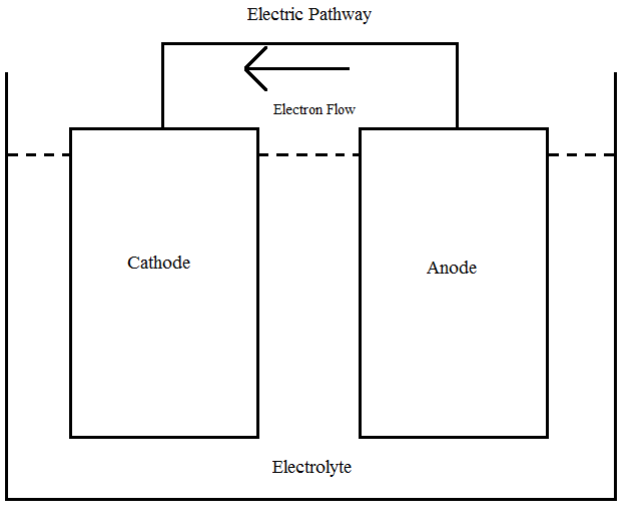

Figure 1.1: A general example of a galvanic cell including the four basic components.

1.1 Galvanic Corrosion

Galvanic corrosion is caused by two dissimilar metals being in electrical contact [1, 5]. This corrosion is much more severe than a corrosive system consisting of one metal. When a metal is placed in an electrolyte, it corrodes at its own resting potential, or open circuit potential (OCP). When considering a galvanic cell with two dissimilar metals, the metal with the higher OCP is the cathode, and the metal with the lower OCP is the anode. This allows metals to be categorized based on their resting potentials, as seen in Figure 1.2. In our case, we see that aluminum has a lower resting potential than stainless steel, thus making the aluminum plate the anode and the stainless steel fastener the cathode. When two dissimilar metals are surrounded by an electrolyte, there is a potential drop that is caused by one metal having a higher

resting potential. This potential drop is one of the mechanisms that influences the initiation of corrosion.

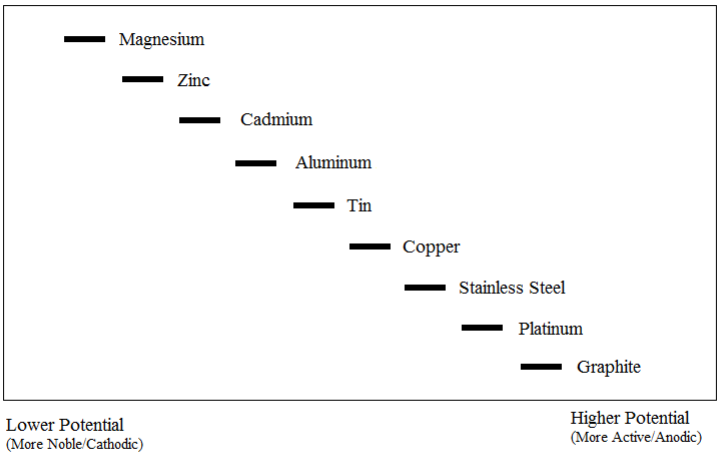

Figure 1.2: Chart demonstrating the nobility of different metals [1].

Galvanic corrosion is influenced by this potential drop. A larger difference between the two resting potential corresponds to a larger flow of electrons, or a larger current. This results in more severe corrosion because the anode dissolves faster due to the higher loss of electrons and higher dissolution rates. This drop is often referred to as the IR drop (from Ohm's law $E = IR$), and galvanic corrosion is said to be IR driven [1], where E is the potential, I is the current, and R is the resistance.

Because electrons are negatively charged, they flow from the metal with the lower OCP to the metal with the higher OCP. Therefore, they travel from the anodic

aluminum to the cathodic stainless steel. This causes dissolution of the aluminum, resulting in the release of aluminum cations into the electrolyte. This process of the anode losing electrons and dissolving is known as an oxidation reaction ($Al \Rightarrow Al^{3+} + 3e^-$). In turn, the cathode gains the electrons lost by the anode resulting in a reduction reaction ($O_2 + 2H_2O + 4e^- \Rightarrow 4OH^-$).

A tool commonly used to investigate and understand galvanic corrosion is a plot of the polarization curves. These curves are experimentally measured and show the relationship between the current density (current per unit length, area, volume) and potential. These curves are very specific to the metal and depend on geometry, length ratio of the anode to cathode, and electrolyte composition. The curves for each individual metal are commonly placed in the same graph to compare them. Figure 1.3 illustrates some general polarization curves for two metals. Each curve has a point where the current density is the lowest. The potential corresponding to this point is the OCP. Therefore, it is easy to tell from the polarization curves which metal is the cathode (higher OCP) and which is the anode (lower OCP). Each curve also has two branches. The lower branch corresponds to the metal being cathodic and the upper branch corresponds to the metal being anodic. The point where the anodic branch of the anode and the cathodic branch of the cathode intersect defines the couple potential, which is the potential value where the metals are in physical contact. At this point in the system, the current density is high, therefore, corrosion rates are high, which has been modeled and observed in experiments [1].

Another important property of the polarization curves is the active-to-passive

transition. Some metals have this transition where the current density spikes as the potential increases. This can be characterized by a "nose", or sudden increase then decrease in the current density on the curve. This identifies a potential range where if the potential transitions into this range, corrosion is initiated and corrosion rates greatly increase. This is referred to as the active-to-passive transition. However, AA7075 does not have this property. Therefore, the initiation of corrosion in aluminum must be caused by some other mechanism, which is discussed later.

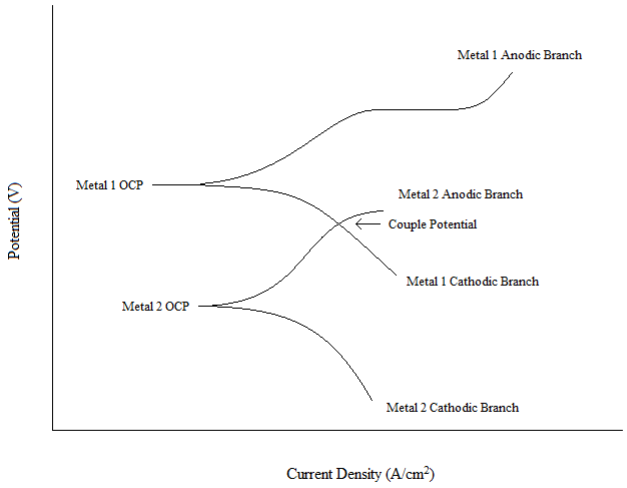

Figure 1.3: A set of general polarization curves illustrating the open circuit potentials and the couple potential.

1.2 Pitting Corrosion

Pitting corrosion is a form of localized corrosion, meaning it only occurs in a small area. It has been observed that this type of corrosion causes a "drilling" effect, severely damaging the metal in the direction normal to the surface of the metal. This effect creates pits, hence the name, that can be either metastable, or stable. Metastable pits are pits that either grow to a few microns in length and then repassivate (stop growing), or become stable [6]. Stable pits are metastable pits that never repassivate in severe environmental conditions (acidity, anion concentration, etc.). Metals with a heterogeneous micro-structure are at high risk of pitting corrosion when exposed to aggressive environments. In particular, Al_7Cu_2Fe, $Al_{23}CuFe_4$, and Al_2CuMg, among other inter-metallic particles, are included in AA7075 [7]. Due to the high number of different metals, AA7075 is highly susceptible to pitting corrosion. Pitting can also become more severe when the metal is present in a galvanic system. A galvanic system causes a larger potential near the mouth, in turn increasing the potential everywhere in the crevice. This increases the chances that the potential in the crevice is above the pitting potential, resulting in higher pitting rates.

Pitting occurs in three stages: passive film breakdown, formation of metastable pits, and the growth of stable pits [6, 8]. Thin oxide layers naturally form on the surface of metal alloys. These layers are passive and greatly reduce the risk of corrosion, helping to protect the metal against the initiation of corrosion. However, these layers are susceptible to breakdown by various means. One of the most common causes of

this breakdown is the presence of an aggressive anion [6, 9, 10]. Most of the time, chloride ions are present and play this role. It has been found that the magnitude of corrosion damage is directly proportional to chloride concentration, implying that the most damage occurs where there is higher a concentration of chloride [8, 11]. This has been observed by Webb and Alkire [12]. When the protective layer is breached, the metal that it previously protected begins to dissolve, causing the initiation of pitting corrosion [6, 8, 10].

The breakdown of the passive film happens extremely quickly and is difficult to observe or measure. In this thesis, we consider this layer to be uniform in species concentration and width, although in reality this is not the case. These layers differ both in chemical composition and shape. There are three main theories as to how the breakdown occurs. The first is film penetration, where the aggressive anion passes through the passive film layer. This phenomenon aids in the accelerated dissolution of the metal. The second theorized breakdown mechanism is adsorption, where the passive film layer is broken down by the aggressive anions over time, allowing them to get to the metal and cause corrosion. The third mechanism is film breaking, which is where the film breaks and allows the anions to pass through [6].

During the second stage of pitting corrosion, metastable pits form. Normally, in order for pits to form, the electric potential has to be greater than a characteristic potential value called the pitting potential [13, 14]. The intermetallic particles in aluminum alloys effectively lower the pitting potential, resulting in a higher risk of corrosion. However, in this stage, metastable pits can form even though the potential

may be below the pitting potential. When a metastable pit forms, there is some remnant of the passive film covering the metastable pit [11, 15]. During this stage, the current density is approximately constant and the growth of the pit is controlled by the ohmic resistance of the cover. Frankel [15] found that if the pit cover bursts too early, the pit will repassivate, but if the cover lasts long enough for a salt film precipitate to form at the pit surface, the pit will become stable.

Pride et al. [16] found that during the initial stages of pitting in aluminum, the current density is constant and many orders of magnitude higher than during the propagation of corrosion. In Chapter II where the aluminum concentration problem is introduced, this idea of a large, constant current density is used when considering the source of aluminum due to metastable pitting.

The last stage of pitting corrosion is the growth of stable pits. The stability of pits and the rate of pit growth depend on electrolyte composition, metal composition, pit potential, acidity, and other factors. The main cause of pits remaining stable is the severity of the electrolyte composition (high anion concentration, high acidity) and the potential in the pit. Webb and Alkire [12] found that an increase in chloride concentration corresponds to a decrease in the pitting potential, making it easier for pitting to occur. Galvele [17] claimed that in order for a metastable pit to become stable, a particular level of acidity in the pit must be realized. It has also been observed that the potential in the pit must be higher than the pitting potential in order to maintain local acidity in the pit [14, 17, 18]. Galvele's main result was that for the acidity to reach the value it needs to initiate pitting, the value of the pit depth

times current density must exceed a critical value. [17].

Other authors also found that a particular current must be reached in order for a pit to become stable [16]. When a metastable pit transitions to a stable pit, the film covering the pit bursts. This causes a sudden drop in the current density. This transition can only occur if the potential is above the pitting potential and the current density is large enough [11].

1.3 Crevice Corrosion

Crevice corrosion is the dissolution of a metal due to severe conditions in a tightly confined area. In this thesis, the crevice is the area between the stainless steel fasteners and the AA7075 plate as seen in Figure 2.4. The width of this crevice is on the order of 100 microns (10^{-4} meters). In order for crevice corrosion to occur, the crevice must be thin enough to capture an aggressive electrolyte composition (contains aggressive anions, oxygen, etc.) and inhibit ion diffusion out of the crevice, but at the same time large enough to allow the electrolyte and ions to enter the crevice. Also, if the crevice is too wide, the ions in solution diffuse out of the crevice easily and the system begins to act like a galvanic system.

As stated before, multi-metallic crevice systems, like the one we are considering here, cause a larger potential drop than systems with one metal. The potential drop resulting from the galvanic couple corresponds to higher currents and accelerates pitting corrosion [19]. The aluminum cations that are released in our system due to pitting cause the aggressive chloride ions to flow into the crevice in order to

satisfy electroneutrality. The chloride then compromises the passive film resulting in higher corrosion rates, creating an auto-catalytic corrosion cell. Due to the fact that aluminum does not have the active-to-passive transition, this is the mechanism that initiates aluminum corrosion.

Crevice corrosion, like pitting, also generally happens in three stages. The first stage is incubation/corrosion initiation. The next stage is propogation of crevice corrosion, and the last stage is repassivation of corrosion or the failure of the system [20, 21]. The initiation stage is where the critical crevice solution is attained. The critical crevice solution is the aggressive environment present at the onset of crevice corrosion, and is characterized by low pH values and high chloride concentrations. The initiation stage is also when oxygen depletion occurs. As oxygen is consumed by reactions in the crevice, it also diffuses into the crevice from the bulk. In most cases, the rate of consumption is higher than the rate of diffusion, which is slow due to the thin geometry of the crevice, and the concentration of oxygen becomes depleted in the crevice. However, because oxygen is still diffusing into the crevice, there is a considerable amount of oxygen towards the mouth of the crevice. By solving for the oxygen concentration in the crevice, we find that the concentration decreases exponentially down the length of the crevice and there is a location which is referred to as the point of deaeration that marks where the oxygen concentration switches from aerated (considerable amount of oxygen) to deaerated (little to no oxygen). In this thesis, we take the point of deaeration to be the location in the crevice where the oxygen concentration at steady-state is 20% of the bulk concentration.

After corrosion initiates, its stability depends on the current provided by the cathode, a sufficiently active anode, and the presence of oxygen. If the cathode cannot provide the current required by the anode to sustain its reactions, corrosion will stop [1, 17]. Also, the anode must be sufficiently active in order to maintain corrosion. If the anode doesn't supply enough cations, the solution will not retain its aggressiveness and corrosion will diminish. So in the final stage, either the system will repassivate and corrosion will stop, or the system will fail due to the damage from corrosion.

1.4 Overview of Problems

As stated above, we solve for the potential, oxygen concentration, and aluminum ion concentration in the crevice, and for the potential in the bulk. Because high chloride ions correspond to high corrosion rates, we are interested in the concentration of chloride ions along the length of the crevice. In order to find the concentration of chloride ions, we solve for the concentration of aluminum ions and use electroneutrality to obtain the chloride. This is simpler because we can make use of the metastable pitting rate to obtain the aluminum. It turns out that the metastable pitting rate depends on chloride and potential, so from this, we are able to calculate the metastable pitting rates of aluminum and determine the influx of aluminum ions in the system. To account for the dependence of aluminum ions on chloride, we lag the chloride concentration and solve for the potential in the crevice. We derive a non-linear, second order differential equation for the potential in the crevice in Chapter II using

the couple potential in a deaerated environment as the boundary condition at the tip of the crevice, and the couple potential in the bulk at the crevice location for the boundary condition at the mouth of the crevice. Also, the potential depends on the polarization curves of both the aluminum and the stainless steel. However, the polarization curves are different in the deaerated zone and the aerated zone, so in order to determine the location where we switch from aerated to deaerated, we need to solve for the oxygen concentration. Therefore, we solve for the potential in the bulk first to obtain the boundary condition at the mouth of the crevice, and solve for the oxygen concentration to determine the point of deaeration. Then using the solutions to these problems, we solve for the potential in the crevice. With this, we can evaluate the source of aluminum due to metastable pitting and solve for the aluminum concentration, thereby giving us the chloride concentration.

1.5 Literature Review

Bulk Potential

Stenta considered two galvanic couple systems [1]. The two couples he considered were aluminum/copper in 0.1 M NaCl solution and magnesium/mild steel in 1.6% NaCl solution. Like the work in this thesis, Stenta assumes a well mixed electrolyte, incompressible fluid flow, and a thin electrolyte film; however, he does not consider a crevice in the system and only takes into account galvanic corrosion. We account for the presence of a crevice by assuming a constant current density over the mouth of the crevice. An asymptotic procedure similar to the one detailed in Chap-

ter II is used to derive a one dimensional equation for the potential in the bulk from the Laplace equation. Unlike the work done here, Stenta does predict the damage profile over time and finds that the current density at the anode/cathode interface spikes, resulting in high corrosion damage. An important result from Stenta [1] is the potential profile. He found that the potential is lower at the anode and higher at the cathode, and is equal to the couple potential at the anode/cathode interface. We expect similar results for the aluminum/steel couple.

In [5], Deshpande makes use of an Arbitrary Lagrangian Eulerian method implemented via COMSOL to predict the damage due to galvanic corrosion. Deshpande considers a magnesium AE44 alloy, mild steel couple and also an AE44, aluminum 6063 alloy couple, and also assumes the electrolyte is well mixed, resulting in the Laplace equation for the potential. Because Deshpande uses COMSOL, it was possible to produce a plot for the potential and damage for a two dimensional domain, instead of the one dimensional domain we use. It was found again that close to the metal/electrolyte interface, the potential is higher at the cathode and decreases monotonically towards the anode.

Oxygen Depletion

Part of Stenta's dissertation [20] solves for the oxygen concentration in a crevice in order to account for deaeration when solving for the potential. The same reaction-diffusion equation included in this thesis was used; however the values of the parameters were different. Stenta considers widths varying from 100 microns to .1

microns. It can be seen in his plots that the smaller the crevice width, the faster and closer to the mouth depletion occurs. The oxygen concentration was also found to be monotonically decreasing down the length of the crevice. We do a similar parameter study investigating the effect of the width and diffusivity on depletion.

Crevice Potential

Hebert and Alkire [22] mathematically modeled crevice corrosion, taking into account the effect dissolution of aluminum has on the initial rapid onset of corrosion, meaning the model is only used for early times before breakdown initiates. A radial crevice was considered, assuming the radius of the crevice is much larger than its height. Hebert and Alkire solved for potential in the crevice assuming the potential at the mouth is equal to that of the bulk, and also solved for various species concentrations including oxygen, chloride ions, and aluminum ions. This was done using a coupled system of equations, whereas in this thesis, the equations are all independent of each other. It was found that the potential was highest at the mouth and decreased monotonically in the inward, radial direction. Likewise, we expect in this thesis to find the potential decreases down the length of the crevice.

Aluminum Ion Concentration

Young [19] investigates a two-year exposure study in Daytona Beach, Florida using aluminum coupons and various metal fasteners. The purpose of the study was to identify corrosion damage modes and develop a sequence of damage stages. The

different fasteners involved in the study were 316L stainless steel, cadmium plated low carbon 1018 steel, and cadmium plated fasteners with the plating partially removed. Young found that severe corrosion was not occurring at the mouth, but rather further down the crevice. This contradicts the argument that because the potential is highest at the mouth, the highest rates of corrosion occur at the mouth. This leads us to believe there is a different, more prominent, cause of corrosion in the crevice. We believe the cause of this is high chloride ion concentrations in the crevice interior due to the maximum aluminum ion concentration being away from the mouth.

Colwell [3] formulated a stochastic, pit initiation model for AA7075 using the kinetic Monte Carlo method, as well as a metastable pit model using a non-homogeneous Poisson process. The metastable pit generation rates were developed as a function of potential and chloride, among other environmental factors. The MATLAB code from Colwell's thesis is used in this thesis to determine metastable pit generation rates as a function of potential and chloride concentration. This implementation is shown Chapter II.

1.6 Thesis Summary

The problems we solve and the order in which we solve them to find the chloride concentration is detailed above in Section 1.4. First, we develop the equations and conditions that we use to solve for the potential, oxygen concentration, and aluminum concentration in Chapter II. In Chapter III, the numerical formulation used to solve these problems numerically is detailed.

CHAPTER II

MODEL FORMULATION

In this thesis, we investigate the mechanisms that lead to the initiation of corrosion in a fastener assembly. We consider two major areas in the geometry: the bulk, which is the boldly exposed surface, and the crevice, which is the thin gap between the fastener and the plate. Figure 2.1 shows the bulk and the crevice. We wish to obtain the chloride ion concentration in the crevice, which would indicate the likely location and severity of corrosion damage. To study the chloride concentration, we solve a reaction-diffusion equation for the aluminum ion concentration in the crevice. Due to electroneutrality, high aluminum ion concentrations correspond to high chloride concentrations. In order to solve for the aluminum ion concentration, the potential in the crevice must be obtained. The reason for this is explained in more detail in Chapter III. Likewise, in order to solve for the potential in the crevice, we need both the potential in the bulk and the oxygen concentration in the crevice. The oxygen concentration is used to determine the point of deaeration in the crevice, which marks the point where we switch from aerated polarization curves to deaerated polarization curves, and the potential in the bulk sets the potential at the mouth of the crevice. Therefore, we formulate and solve the problem for the potential in the bulk first.

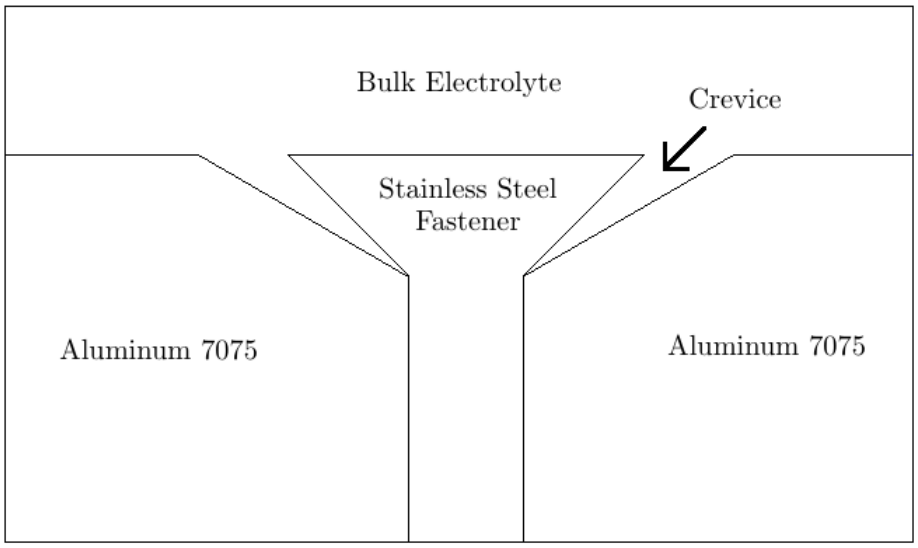

Figure 2.1: The geometry under consideration, showing the separation of the bulk and the crevice.

2.1 Bulk Potential

The problems for the potential in the bulk and in the crevice are derived using the same method. We start by deriving an equation for the potential from the general mass transport equation. For future reference, this derivation is done for all time, although we are only concerned about initial time in this work.

2.1.1 Bulk Potential Formulation

We start with the general mass transport equation, which is given by

$$\frac{\partial C_i}{\partial t} = -\nabla \cdot \mathbf{J_i}, \tag{2.1}$$

where C_i is the concentration of species i and $\mathbf{J_i}$ is the flux vector of species i. We write $\mathbf{J_i}$ as

$$\mathbf{J_i} = -D_i \nabla C_i - \frac{Z_i D_i F_a C_i}{RT} \nabla E + C_i \mathbf{v}, \tag{2.2}$$

where D_i is the diffusion coefficient of species i, Z_i is the number of valence electrons in species i, $\mathbf{v}$ is the fluid velocity vector, R is the universal gas constant, E is the potential, and T is the temperature in Kelvin of the electrolyte, which we are assuming to be constant. There are three main transport mechanisms. The first term in (2.2) corresponds to diffusion of the species, the second term represents migration, and the final term represents convection.

Because we assume the electrolyte is well mixed, meaning all species concentrations are spatially uniform, the gradients are equal to zero, meaning

$$\nabla C_i = 0.$$

Also, we assume the flow of the electrolyte is incompressible, meaning the density of the fluid remains constant. This implies that the divergence of the fluid velocity, $\nabla \cdot \mathbf{v}$, is zero. With these two assumptions, the transport equation becomes

$$\frac{\partial C_i}{\partial t} = \nabla \cdot \Big[\frac{Z_i D_i F_a C_i}{RT} \nabla E \Big]. \tag{2.3}$$

All of the species must obey electroneutrality. This means the sum of the charges of the ions in the electrolyte must balance to zero. Therefore, we have

$$\sum_i Z_i C_i = 0. \tag{2.4}$$

Differentiating equation (2.4) with respect to time and using equation (2.3) to substitute for $\partial C_i/\partial t$ gives

$$\frac{\partial}{\partial t}\sum_i Z_i C_i = \sum_i Z_i \frac{\partial C_i}{\partial t} = \sum_i \nabla \cdot \Big[\frac{Z_i^2 D_i F_a C_i}{RT}\nabla E\Big] = 0. \tag{2.5}$$

Using the product rule to expand (2.5), we get

$$\sum_i \frac{Z_i^2 D_i F_a}{RT}(\nabla C_i \nabla E + C_i \nabla^2 E) = \nabla^2 E \sum_i \frac{Z_i^2 D_i F_a}{RT} C_i = 0. \tag{2.6}$$

Because the parameters, constants, and species concentrations are all greater than 0, implying the sum in the right hand side of (2.6) is non-zero, we obtain

$$\nabla^2 E = 0.$$

This is the governing equation for the potential that we use to derive a more simple equation to solve for the potential in the bulk and in the crevice. Denote the bulk potential as E_b and the potential in the crevice as E_{cr}. Also denote the damage in the bulk as $H_b(x,t)$ and the damage in the crevice as $H_{cr}(x,t)$.

With this, the problem for the potential in the bulk is

$$\begin{aligned}
\nabla^2 E_b &= 0, && (2.7)\\
\frac{\partial E_b}{\partial x}(0,y,t) &= 0, && (2.8)\\
\frac{\partial E_b}{\partial x}(L_b,y,t) &= 0, && (2.9)\\
\frac{\partial E_b}{\partial y}(x,w_b,t) &= 0, && (2.10)\\
-\kappa \nabla E_b \cdot \hat{n} &= i(E_b), \qquad y = -H_b(x,t), && (2.11)
\end{aligned}$$

where the geometry is shown in Figure 2.2, and the function H_b is shown in Figure 2.3. Here, L_b is the length of the surface domain, w_b is the width of the bulk electrolyte, κ

is the conductivity of the electrolyte, $\hat{n}$ is the outward normal vector to the boundary $y = -H_b$, and $i(E_b)$ is the current density along the boundary $y = -H_b$. Here, $i(E_b)$ is given by

$$i(E_b) = \begin{cases} i_{ca}(E_b), & x \leq p_1, \\ i_{fixed}, & p_1 < x < p_2, \\ i_{aa}(E_b), & x \geq p_2, \end{cases}$$

where i_{aa} is the aerated current density of the anode, i_{fixed} is the current density at the mouth of the crevice, and i_{ca} is the aerated current density of the cathode. The value of i_{fixed} is unknown. Brackman [4] was able to determine the value of the potential at the mouth by using a bisection method until potential flux was equal to 0. From this we could determine the value of i_{fixed}, but instead we simply test different values to determine the effect of i_{fixed} on the potential. The current densities i_{aa} and i_{ca} are obtained from the aerated polarization curves. In this thesis, we use the set from Liu et al. [23].

The value p_1 is the location of the anode/crevice interface, and p_2 is the location of the crevice/cathode interface, which is illustrated in Figure 2.2. We also wish to take advantage of the symmetry of the geometry by only considering one side of the fastener. At $x = 0$, there is no potential flux due to the symmetry of the geometry. At $x = L_b$ and $y = w_b$, we assume there is no potential flux in the far field. The condition at $y = -H_b(x, t)$ is derived from Ohm's Law. The outward normal

vector to $y = -H_b(x,t)$ is given by

$$\hat{n} = \frac{\nabla F}{||\nabla F||} = \frac{\left\langle -\dfrac{\partial H_b}{\partial x}, -1 \right\rangle}{\sqrt{1 + \left(\dfrac{\partial H_b}{\partial x}\right)^2}},$$

where $||\cdot||$ denotes the Euclidean norm of a vector, and F is the surface defined by $F = -y - H_b = 0$. So the boundary condition on $y = -H_b$ becomes

$$\frac{\dfrac{\partial E_b}{\partial x}\dfrac{\partial H_b}{\partial x} + \dfrac{\partial E_b}{\partial y}}{\sqrt{1 + \left(\dfrac{\partial H_b}{\partial x}\right)^2}} = \frac{i(E_b)}{\kappa}, \qquad y = -H_b.$$

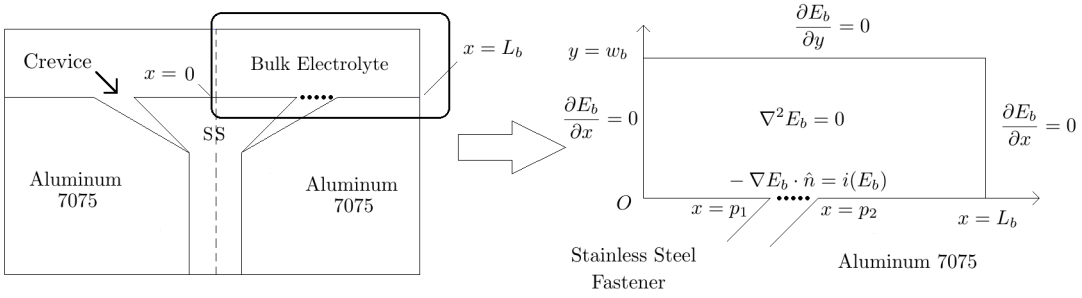

Figure 2.2: Domain for the bulk potential problem. The cathodic aerated current density, i_{ca}, is used between $x = 0$ and $x = p_1$, the fixed current density, i_{fixed}, is used between $x = p_1$ and $x = p_2$, and the cathodic aerated current density, i_{aa}, is used between $x = p_2$ and $x = L_b$.

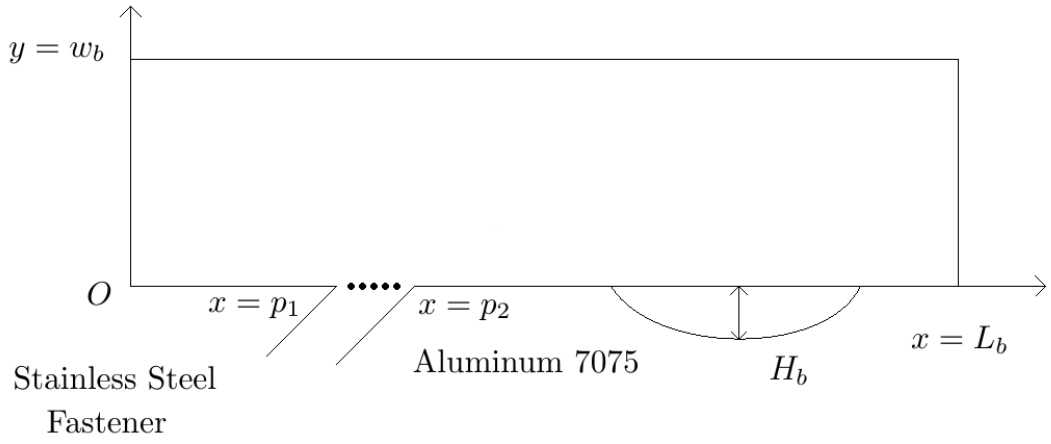

Figure 2.3: Illustration of the function H_b.

2.1.2 Bulk Potential Asymptotic Procedure

In order to obtain the final equation for the potential in the bulk, we use an asymptotic procedure to take advantage of the disparity in length scales of the thin domain, and reduce the problem to a second order, ordinary differential equation. We start by non-dimensionalizing equation (2.7). We use the scalings shown in Table 2.1. The values E^* and i^* are some characteristic potential and current density, respectively. The value of E^* could take on the pitting potential, the couple potential, or the OCP. The value of i^* could be the maximum current density on the polarization curves. For our purposes, these values do not matter due to the fact that they cancel out when redimensionalizing the problem. With these scalings, equation (2.7) becomes

$$\frac{E^*}{L_b^2}\frac{\partial \bar{E}_b}{\partial \bar{x}^2} + \frac{E^*}{w_b^2}\frac{\partial \bar{E}_b}{\partial \bar{y}^2} = 0, \tag{2.12}$$

Table 2.1: Scalings for the Potential Equation

Variable	**Units**	**Scaling**	**Non-dimensional Variable**
x	Length (cm)	L_b	$\bar{x}$
y	Length (cm)	w_b	$\bar{y}$
E_b	Volts (V)	E^*	$\bar{E_b}$
H_b	Length (cm)	w_b	$\bar{H_b}$
i	Current Density $\frac{\text{A}}{\text{cm}^3}$	i^*	$\bar{i}$

so that

$$\Big(\frac{w_b^2}{L_b^2}\Big)\frac{\partial \bar{E_b}}{\partial \bar{x}^2} + \frac{\partial \bar{E_b}}{\partial \bar{y}^2} = 0. \tag{2.13}$$

Define $\epsilon = w_b/L_b$. We assume that because the film of electrolyte from the atmosphere is so thin that $w_b << L_b$, implying that $\epsilon << 1$. With this, (2.13) can be written as

$$\epsilon^2\frac{\partial \bar{E_b}}{\partial \bar{x}^2} + \frac{\partial \bar{E_b}}{\partial \bar{y}^2} = 0. \tag{2.14}$$

Similarly, non-dimensionalizing the boundary conditions (2.8)-(2.11) yields

$$\frac{\partial \bar{E_b}}{\partial \bar{x}} = 0, \qquad \bar{x} = 0,\ 1 \tag{2.15}$$

$$\frac{\partial \bar{E_b}}{\partial \bar{y}} = 0, \qquad \bar{y} = 1 \tag{2.16}$$

$$\frac{\epsilon^2\dfrac{\partial \bar{E_b}}{\partial \bar{x}}\dfrac{\partial \bar{H_b}}{\partial \bar{x}} + \dfrac{\partial \bar{H_b}}{\partial \bar{y}}}{\sqrt{1+\epsilon^2\Big(\dfrac{\partial \bar{H_b}}{\partial \bar{x}}\Big)^2}} = \frac{w_b i^*}{\kappa E^*}\bar{i}(\bar{E_b}), \qquad \bar{y} = -\bar{H_b}(\bar{x}, t). \tag{2.17}$$

Using the binomial theorem to expand the square root in the denominator, the condition becomes

$$\Big(\epsilon^2\frac{\partial\bar{E}_b}{\partial\bar{x}}\frac{\partial\bar{H}_b}{\partial\bar{x}}+\frac{\partial\bar{E}_b}{\partial\bar{y}}\Big)\Big(1-\frac{\epsilon^2}{2}\Big(\frac{\partial\bar{H}_b}{\partial\bar{x}}\Big)^2+\frac{3\epsilon^4}{8}\Big(\frac{\partial\bar{H}_b}{\partial\bar{x}}\Big)^4-\cdots\Big)=W\bar{i}(\bar{E}_b), \tag{2.18}$$

with $W=\dfrac{w_b i^*}{\kappa E^*}$. This group of parameters is known as the Wagner number. For systems with a large conductivity or steep polarization curves, the width of the electrolyte (or crevice) is much smaller than the conductivity times the slope of the polarization curve ($w<\kappa\Delta E/\Delta i$) [4]. Therefore, the assumption that $wE^*/\kappa i^* << 1$ is valid, so we assume that $W=O(\epsilon^2)$. We define $W=\gamma\epsilon^2$, where γ is an $O(1)$ constant. Assume the asymptotic expansions $\bar{E}_b=\sum_{k=0}^{\infty}\epsilon^{2k}\bar{E}_{bk}$, $\bar{H}_b=\sum_{k=0}^{\infty}\epsilon^{2k}\bar{H}_{bk}$, and $\bar{i}(\bar{E}_b)=\sum_{k=0}^{\infty}\epsilon^{2k}\bar{i}_k(\bar{E}_b)$. Plugging these expansions into equation (2.14) and boundary conditions (2.15) and (2.16), we get

$$\epsilon^2\sum_{k=0}^{\infty}\epsilon^{2k}\frac{\partial^2\bar{E}_{bk}}{\partial x^2}+\sum_{k=0}^{\infty}\epsilon^{2k}\frac{\partial^2\bar{E}_{bk}}{\partial y^2} = 0, \tag{2.19}$$

$$\sum_{k=0}^{\infty}\epsilon^{2k}\frac{\partial\bar{E}_{bk}}{\partial x} = 0, \qquad \bar{x}=0,\ 1, \tag{2.20}$$

$$\sum_{k=0}^{\infty}\epsilon^{2k}\frac{\partial\bar{E}_{bk}}{\partial y} = 0, \qquad \bar{y}=1. \tag{2.21}$$

Due to the complexity of condition (2.18), the details of the substitution are not shown, and only the resulting conditions for $O(1)$ and $O(\epsilon^2)$ are shown. To obtain these conditions, we substitute the asymptotic expansions into condition (2.18). Then, because the condition is at $\bar{y}=-\bar{H}_b=-\sum_{k=0}^{\infty}\epsilon^{2k}\bar{H}_{bk}$, we plug this into all $\bar{E}_{bk}(\bar{x},\bar{y},t)$ terms and perform a Taylor Series expansion in $\bar{y}$.

To get the first order problem, we consider only the $O(1)$ terms in (2.19)-(2.21) and also the resulting condition from (2.18). This yields

$$\frac{\partial^2 \bar{E}_{b0}}{\partial \bar{y}^2} = 0, \tag{2.22}$$

$$\frac{\partial \bar{E}_{b0}}{\partial \bar{x}}(0, \bar{y}, t) = 0, \tag{2.23}$$

$$\frac{\partial \bar{E}_{b0}}{\partial \bar{x}}(1, \bar{y}, t) = 0, \tag{2.24}$$

$$\frac{\partial \bar{E}_{b0}}{\partial \bar{y}}(\bar{x}, 1, t) = 0, \tag{2.25}$$

$$\frac{\partial \bar{E}_{b0}}{\partial \bar{y}} = 0, \qquad \bar{y} = -\bar{H}_{b0}. \tag{2.26}$$

Integrating (2.22) with respect to $\bar{y}$ twice results in the solution

$$\bar{E}_{b0} = A(x,t)\bar{y} + B(x,t),$$

where $A(x,t)$ and $B(x,t)$ are arbitrary functions to be determined. For ease of notation we suppress the time dependence in what follows. Using conditions (2.23)-(2.26), we get

$$A(x) = 0,$$

$$B_{\bar{x}}(0) = B_{\bar{x}}(1) = 0,$$

$$\bar{E}_{b0} = B(x).$$

In order to find $B(x)$, we must go to the $O(\epsilon^2)$ problem. Taking only the $O(\epsilon^2)$ terms

in (2.19)-(2.21) and the condition at $\bar{y} = -\bar{H}_b$, we get

$$\frac{\partial^2 \bar{E}_{b1}}{\partial \bar{y}^2} = -\frac{\partial^2 \bar{E}_{b0}}{\partial \bar{x}^2} = -B_{\bar{x}\bar{x}}, \tag{2.27}$$

$$\frac{\partial \bar{E}_{b1}}{\partial \bar{x}}(0, \bar{y}, t) = 0, \tag{2.28}$$

$$\frac{\partial \bar{E}_{b1}}{\partial \bar{x}}(1, \bar{y}, t) = 0, \tag{2.29}$$

$$\frac{\partial \bar{E}_{b1}}{\partial \bar{y}}(\bar{x}, 1, t) = 0, \tag{2.30}$$

$$B_{\bar{x}} \frac{\partial \bar{H}_{b0}}{\partial \bar{x}} + \frac{\partial \bar{E}_{b1}}{\partial \bar{y}}(\bar{x}, -\bar{H}_{b0}, t) \;\; = \;\; \gamma \bar{i}_0(\bar{E_{b0}}). \tag{2.31}$$

Again, condition (2.31) comes from the condition at $\bar{y} = -\bar{H}_b$, keeping in mind that $\partial \bar{E}_{0b}/\partial y = B_{\bar{y}} = 0$. Integrating (2.27) with respect to $\bar{y}$ once, we get

$$\frac{\partial \bar{E}_{b1}}{\partial \bar{y}} = -B_{\bar{x}\bar{x}}\bar{y} + C(x).$$

Using the condition at $\bar{y} = 1$, we get $C(x) = B_{\bar{x}\bar{x}}$, which results in

$$\frac{\partial \bar{E}_{1b}}{\partial \bar{y}} = -B_{\bar{x}\bar{x}}\bar{y} + B_{\bar{x}\bar{x}}.$$

And finally, condition (2.31) gives us the non-dimensional version of the equation we will ultimately solve numerically to obtain the potential:

$$B_{\bar{x}} \frac{\partial \bar{H}_{0b}}{\partial x} + B_{\bar{x}\bar{x}}\bar{H}_{b0} + B_{\bar{x}\bar{x}} = \Big[B_{\bar{x}}(1 + \bar{H})\Big]_{\bar{x}} = \gamma \bar{i}_0(\bar{E}_{b0}),$$

$$B_{\bar{x}}(0) = B_{\bar{x}}(1) = 0.$$

The redimensionalized potential equation and conditions are

$$\kappa\Big[(w_b + H_b)\frac{\partial E_b}{\partial x^2}\Big]_x = i(E_b),$$

$$\frac{\partial E_b}{\partial x}(0) = \frac{\partial E_b}{\partial x}(L_b) = 0.$$

Now we have an ordinary, non-linear differential equation for E_b in the x direction. This implies that at leading order, the potential does not vary in the y direction. For early time, the damage due to corrosion is minuscule. Because of this, we can simplify the problem by using $H_b = 0$. This gives us the equation for E_b at early time,

$$w_b \kappa \frac{\partial^2 E_b}{\partial x^2} = i(E_b), \tag{2.32}$$

$$\frac{\partial E_b}{\partial x}(0,t) = \frac{\partial E_b}{\partial x}(L_b,t) = 0. \tag{2.33}$$

Equation (2.32) with corresponding boundary conditions (2.33) is solved to get the potential in the bulk.

2.2 Oxygen Concentration Problem

When considering the solution to the potential problem in the crevice, we must consider the point along the crevice where the electrolyte becomes deaerated so we can switch from aerated polarization curves to deaerated curves at the appropriate location. We arbitrarily consider the point of deaeration to be the location in the crevice where the oxygen concentration is 20% of the bulk concentration. In order to determine where this occurs, we solve the following reaction-diffusion problem:

$$u_t = D_O u_{xx} - \frac{i_O}{4 w_{cr} F_a}\Big(\frac{u}{O_{2bulk}}\Big), \tag{2.34}$$

$$u(0,t) = O_{2bulk}, \tag{2.35}$$

$$u(x,0) = O_{2bulk}, \tag{2.36}$$

$$\frac{\partial u}{\partial x}(L_{cr},t) = 0. \tag{2.37}$$

Here, u is the concentration of oxygen in the crevice, D_O is the diffusion coefficient for oxygen, i_O is the approximate current density associated with the oxygen depletion, and O_{2bulk} is the fixed concentration of oxygen in the bulk electrolyte. The oxygen transport is governed by diffusion, which is represented by the first term on the right hand side. The second term on the right hand side is a sink term derived from Faraday's Law that takes into account the reactions in the system that consume oxygen. The O_2 concentration at the mouth of the crevice must equal the concentration in the bulk, so at the mouth of the crevice, u is set to the bulk concentration. Initially, the reactions that consume oxygen have not yet begun, so the initial oxygen concentration along the length of the crevice is the same as the bulk concentration. Finally, because oxygen is unable to transport through the tip of the crevice, the flux of u is set to 0 at $x = L_{cr}$. The domain can be seen in Figure 2.4. Note that we do not take the angled bend of the crevice into account, so x is not a coordinate, but is defined as the length down the crevice.

As time increases, the oxygen is used up. Oxygen from the bulk replaces the oxygen consumed by reactions over time. However, it is more difficult for the oxygen to transport down the crevice because the crevice is so thin. Because of this, we expect the concentration to monotonically decrease over time and space within the crevice. We solve the oxygen problem both numerically using MATLAB and analytically using eigen-function expansions. The analytic solution procedure is detailed in Appendix **??** and is used to validate the solution of the numerical solution.

Although we are only concerned with early time solutions, we include time

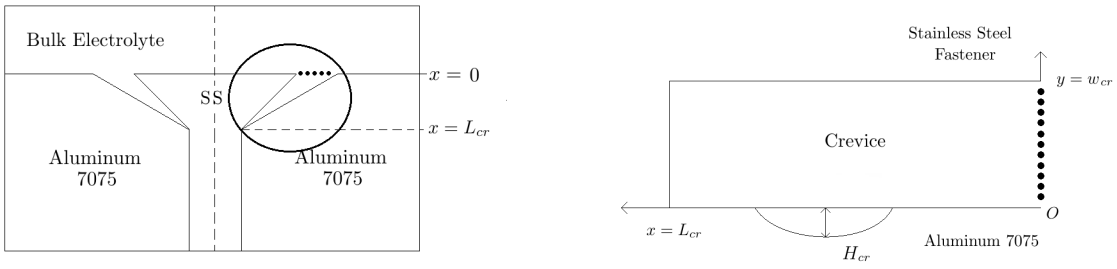

Figure 2.4: The crevice region in relation to the total geometry. The dots show the connection between the bulk and the crevice. A zoomed in view of the crevice is on the right, where x is the length down the crevice. To simplify the problem, we consider a rectangular domain. This view has been rotated with the steel at the top and the aluminum at the bottom.

in this formulation. The reason for this is because the amount of time it takes for the oxygen to deplete and reach steady state is much faster than the initial stage of corrosion damage evolution. Therefore, it is desirable to use the steady state solution because the point of deaeration is constant by the time corrosion initiates.

2.3 Crevice Potential Problem

The procedure we use to formulate the problem for the potential in the crevice is almost identical to the procedure we use for the bulk potential problem. The only difference is the definition of the current density and the boundary conditions. The

initial, two-dimensional problem for the crevice potential is

$$\nabla^2 E_{cr} = 0, \tag{2.38}$$

$$E_{cr}(0, y, t) = E_{mouth}, \tag{2.39}$$

$$E_{cr}(L_{cr}, y, t) = E_{tip}, \tag{2.40}$$

$$-\kappa \nabla E_{cr} \cdot \hat{n} = i_a(E_{cr}), \qquad y = -H_{cr}(x, t), \tag{2.41}$$

$$-\kappa \nabla E_{cr} \cdot \hat{n} = -i_c(E_{cr}), \qquad y = w_{cr}. \tag{2.42}$$

Here, $i_a(E_{cr})$ is the anodic current density in the crevice, $i_c(E_{cr})$ is the cathodic current density in the crevice, E_{mouth} is the potential at the mouth of the crevice which is obtained from the bulk potential solution, E_{tip} is the potential at the tip of the crevice due to the deaerated couple, L_{cr} is the length of the crevice, and w_{cr} is the width of the crevice. The couple potential values at the tip and mouth are used for E_{tip} and E_{mouth} respectively. Again, Figure 2.4 shows the crevice geometry. The transition between aerated and deaerated zones is modeled by

$$i_a(E_{cr}) = \alpha(x) i_{aa}(E_{cr}) + (1 - \alpha(x)) i_{ad}(E_{cr}),$$

$$i_c(E_{cr}) = \alpha(x) i_{ca}(E_{cr}) + (1 - \alpha(x)) i_{cd}(E_{cr}),$$

where i_{aa} is the anodic, aerated current density, i_{ad} is the anodic, deaerated current density, i_{ca} is the cathodic, aerated current density, i_{cd} is the cathodic, deaerated current density. As stated in the introduction, the depletion of oxygen due to reduction reactions changes the current density, which is simulated by $\alpha(x)$.

The function α marks the point of deaeration and is a smooth function that is 1 towards the mouth and 0 towards the tip as shown in Figure 2.5. The function

used for $\alpha(x)$ is given by

$$\alpha(x) = -\frac{1}{2}\tanh(200(x - x_d)) + \frac{1}{2},$$

where x_d is the point of deaeration found in the solution to the oxygen depletion problem. The plot of $\alpha(x)$ is shown in Figure 2.5. The function $\alpha(x)$ allows the current density to switch continuously from aerated curves to deaerated curves at the appropriate location based on our results from solving the oxygen depletion problem shown later in the thesis.

Using an argument similar to the bulk problem, the boundary conditions at the y boundaries, (2.41) and (2.42), are equivalent to

$$\begin{aligned} \frac{\frac{\partial E_{cr}}{\partial x}\frac{\partial H_{cr}}{\partial x} + \frac{\partial E_{cr}}{\partial y}}{\sqrt{1 + \left(\frac{\partial H_{cr}}{\partial x}\right)^2}} &= \frac{i_a(E_{cr})}{\kappa}, \qquad y = -H_{cr}, \\ \frac{\partial E_{cr}}{\partial y} &= \frac{-i_c(E_{cr})}{\kappa}, \qquad y = w_{cr}. \end{aligned} \tag{2.43}$$

In this case, both $y = w_{cr}$ and $y = -H_{cr}(x,t)$ are reactive surfaces, giving the conditions on the y boundaries. We then use an asymptotic procedure on (2.38)-(2.43) similar to the one used for the bulk potential problem. We use the scalings shown in Table 2.2.

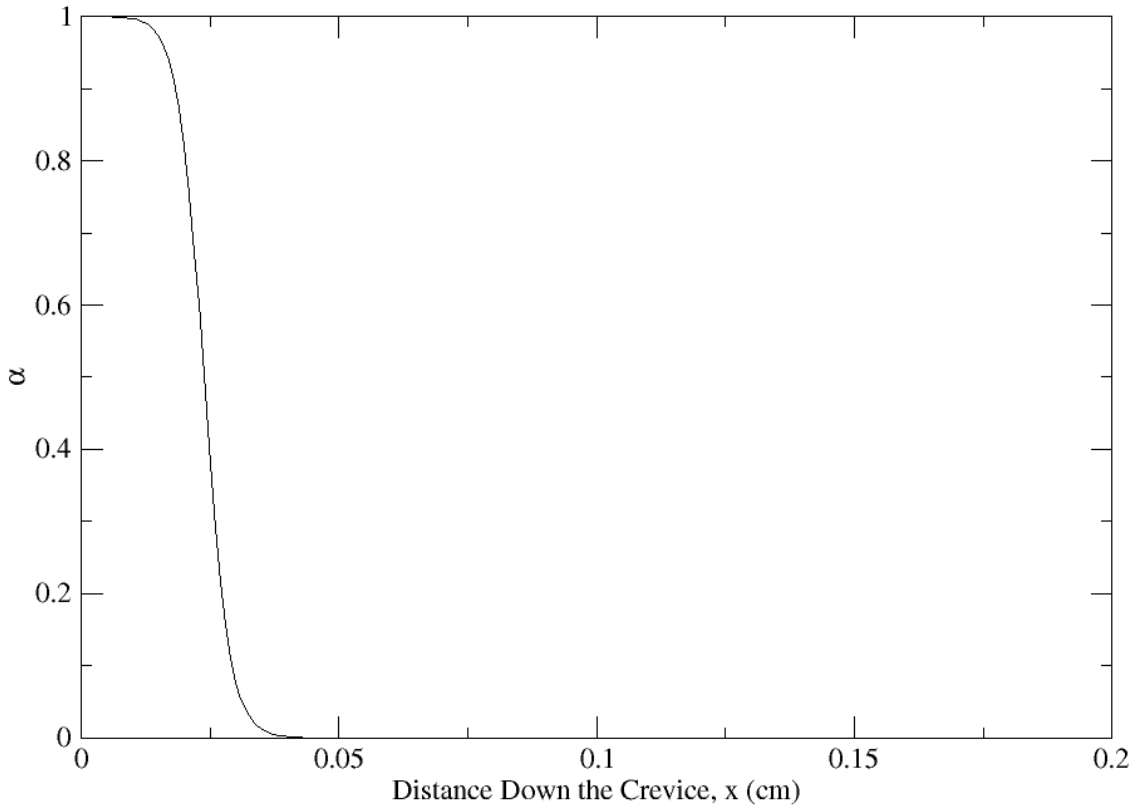

Figure 2.5: Plot of the function $\alpha(x)$, given by $\alpha(x) = -\frac{1}{2}\tanh(200(x - x_d)) + \frac{1}{2}$. The aerated zone is to the left (near the crevice mouth), and the deaerated zone is to the right (deeper into the crevice).

Table 2.2: Scalings for the Potential Equation in the Crevice

Variable	**Units**	**Scaling**	**New Variable**
x	Length (cm)	L_{cr}	$\bar{x}$
y	Length (cm)	w_{cr}	$\bar{y}$
E_{cr}	Potential (V)	E^*	$\bar{E}_{cr}$
H_{cr}	Length (cm)	w_{cr}	$\bar{H}_{cr}$
i	Current Density $\frac{\text{A}}{\text{cm}^3}$	i^*	$\bar{i}$

These scalings result in the following problem:

$$\epsilon^2 \frac{\partial^2 \bar{E}_{cr}}{\partial x^2} + \frac{\partial^2 \bar{E}_{cr}}{\partial y^2} = 0, \tag{2.44}$$

$$\frac{\partial \bar{E}_{cr}}{\partial x}(0, \bar{y}, t) = \frac{\partial \bar{E}_{cr}}{\partial x}(1, \bar{y}, t) = 0, \tag{2.45}$$

$$\frac{\epsilon^2 \frac{\partial \bar{E}_{cr}}{\partial x}\frac{\partial \bar{H}_{cr}}{\partial x} + \frac{\partial \bar{E}_{cr}}{\partial y}}{\sqrt{1 + \epsilon^2 \left(\frac{\partial \bar{H}_{cr}}{\partial x}\right)^2}} = \frac{w_{cr} i^*}{\kappa E^{**}} \bar{i}(\bar{E}), \qquad \bar{y} = -\bar{H}_{cr}(\bar{x}, t). \tag{2.46}$$

Using a similar asymptotic procedure to the bulk problem, we get the following equation:

$$\kappa \Big[\frac{\partial E_{cr}}{\partial x}(w_{cr} + H_{cr}) \Big]_x = i_a(E_{cr}) - i_c(E_{cr}), \tag{2.47}$$

$$E_{cr}(0) = E_{mouth}, \tag{2.48}$$

$$E_{cr}(L_{cr}) = E_{couple}. \tag{2.49}$$

Identical to the bulk problem, we use $H_{cr} = 0$ at early time, turning (2.47) into

$$w_{cr}\kappa\frac{\partial^2 E_{cr}}{\partial x^2} = i_a(E_{cr}) - i_c(E_{cr}). \tag{2.50}$$

2.4 Aluminum Ion Concentration Problem

To obtain the aluminum ion concentration, we solve the reaction diffusion equation with a source that corresponds to the pitting of aluminum. The problem we solve is

$$\frac{\partial C}{\partial t} = D_A\frac{\partial^2 C}{\partial x^2} + \frac{i_A(x,t)}{Zw_{cr}F_a}, \tag{2.51}$$

$$C(0,t) = C(x,0) = Al_{bulk}, \tag{2.52}$$

$$\frac{\partial C}{\partial x}(L_{cr},t) = 0. \tag{2.53}$$

The function $i_A(x,t)$ is given by

$$i_A(x,t) = i_{A,constant}\frac{\rho(E,[Cl^-])}{\max\limits_x\{\rho(E,[Cl^-])\}},$$

where $i_{A,constant}$ is the initial time current density associated with metastable pitting, and ρ is the metastable pitting rate dependent upon the potential and chloride ion concentration at x. We note the form of ρ is taken from Colwell [3]. As mentioned in the introduction, Pride et al. [16] found that during the initial stages of pitting in aluminum, the current density is constant and on the order of magnitude of 1 A/cm^2. The range of current densities found for the range of potential values in the crevice we are considering is from about 0.05 to 1 A/cm^2. In this thesis, various $i_{A,constant}$ values within this range are used to study the effect of the initial current density on the aluminum ion concentration.

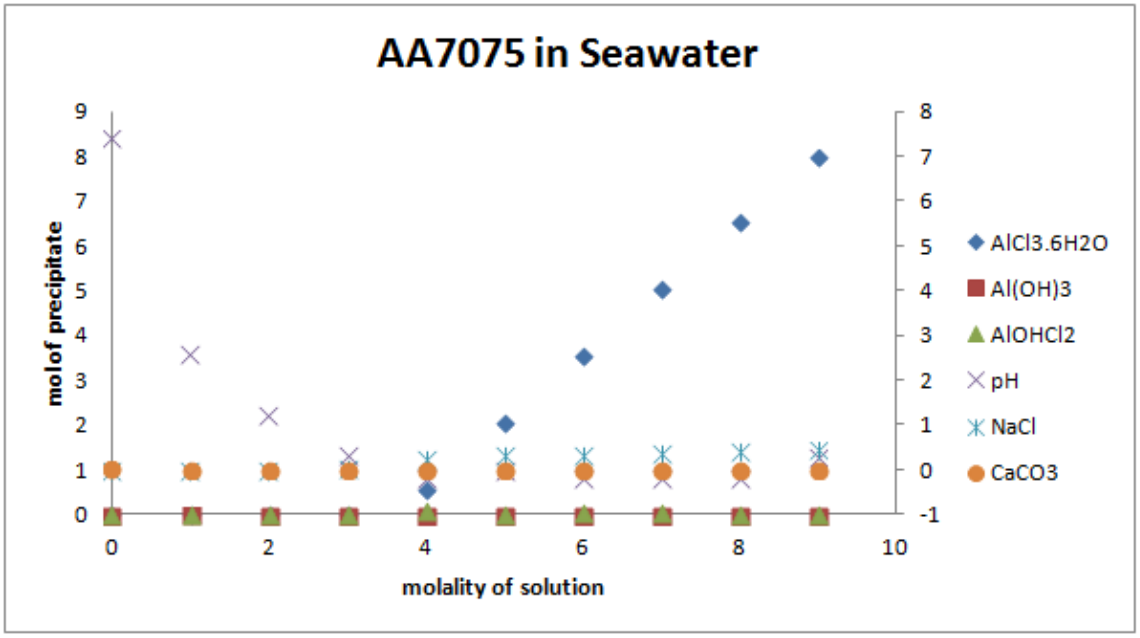

Figure 2.6: The results from Lillard's [2] OLI calculations. It can be seen from the graph that if the aluminum concentration is less than or equal to 3 M, then there are no aluminum salt precipitates.

This equation for aluminum ion concentration does not account for the loss of aluminum due to reactions in the electrolyte. These reactions form salt precipitates. It has been observed in OLI calculations performed by Lillard [2] that there is a threshold value of aluminum concentration where concentrations below this threshold result in no salt formation. As shown in Figure 2.6, this threshold value is at least 3 M. It is shown later that the aluminum concentration does not exceed this threshold, justifying the exclusion of these reactions from the equation.

The function, $i_A(x,t)$, was used to reflect the idea that at locations in the crevice of high corrosion rates, more aluminum ions are produced than aluminum

ions produced at sites of low corrosion rates. At the site of highest metastable pitting rates, $\rho(x) = \max_x(\rho(x))$, making $i_A = i_{A,constant}$. At sites of low corrosion rates, the ratio of $\rho(x)$ to $\max_x(\rho(x))$ is small, meaning i_A is small, which properly reflects the low production of aluminum ions. In order to obtain ρ, we use the code Colwell [3] used to obtain the metastable pit generation rates as a function of chloride and potential, as discussed in Chapter I. A three dimensional table of values that took the potential and chloride ion concentration as inputs and output the metastable pitting rate is created from the code. We then interpolate the table in order to obtain metastable pit generation rates (ρ) for any chloride and potential. Figure 2.7 shows a plot of the interpolation of the table generated by Colwell's code. Note that the method we use to investigate the location and severity of the damage is to solve for the chloride concentration using electroneutrality; however we need the aluminum to calculate the chloride concentration. The way we account for this is to first use the assumption that initially, the aluminum concentration is 0 and the electrolyte is a 0.1 M NaCl solution. This gives us an initial chloride concentration. Then, using this to solve for the aluminum concentration at the next time step, we can use electroneutrality to solve for the chloride at the next time step. So we are lagging the chloride concentration. The equation we use to obtain the chloride concentration is

$$3[Al^{3+}] - [Cl^-] + [Na^+] = 0, \tag{2.54}$$

where the concentration of sodium is constant at 0.1 M. This is to take into account the initial 0.1 M NaCl solution. For simplicity, we do not consider any other species,

and as stated earlier, there is no loss of chloride due to the absence of salt precipitates.

Using the solution for potential in the crevice that was obtained from (2.47)-(2.49) and the chloride concentration, obtained by utilizing electroneutrality, we obtain values for ρ at any x and t value by interpolating the table and creating a surface that can be evaluated at any point, as seen in Appendix **??**.

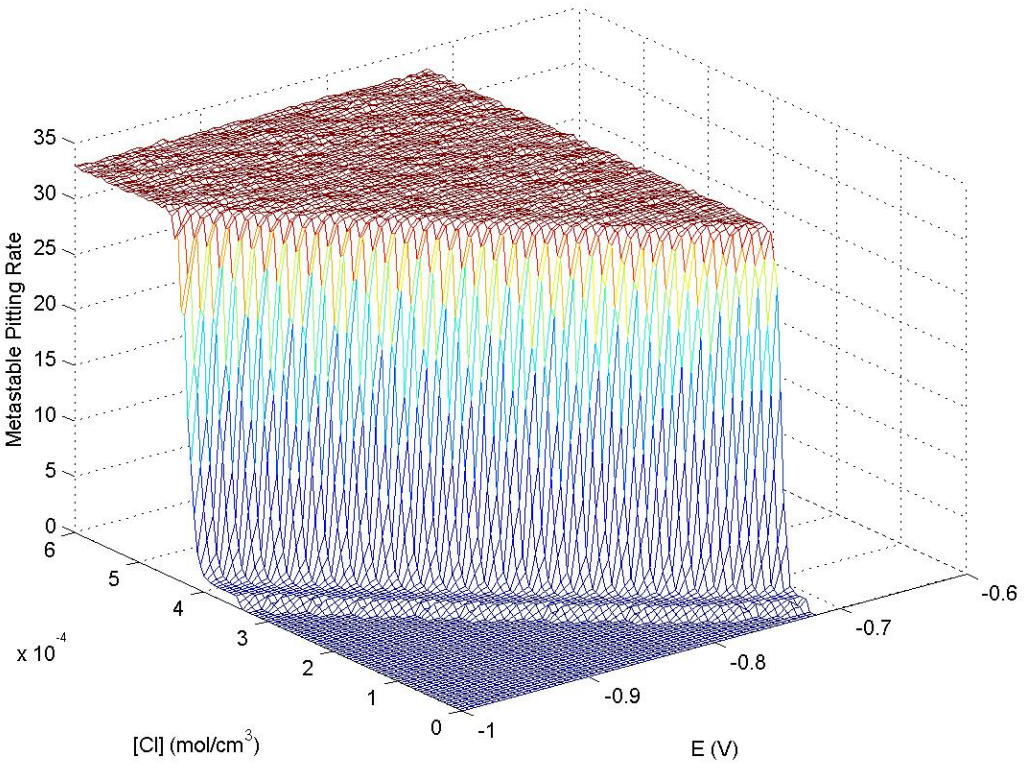

Figure 2.7: Metastable pit generation rate as a function of potential and chloride ion concentration [3].

2.5 Overall Algorithm

As detailed above, there are other environmental aspects we need in order to obtain the aluminum ion concentration, which in turn describes the chloride ion concentration. The idea is to solve for the potential in the bulk so we can obtain the potential at the mouth and solve the oxygen concentration problem in the crevice to determine the point of deaeration in the crevice so we know where to switch from aerated to deaerated polarization curves. Then, we use these two results to solve for the potential in the crevice, and using the potential in the crevice and an interpolation scheme to get ρ from Colwell's metastable pitting rate table, we can solve for the aluminum ion concentration. All of this is done only for the initial stages of corrosion.

CHAPTER III

NUMERICAL FORMULATION

In order to solved the problems for potential, oxygen concentration, and aluminum ion concentration, we use MATLAB. The boundary value problems for the bulk and crevice are solved using the bvp4c solver in MATLAB, while the oxygen and chloride ion concentration problems are solved using the Crank-Nicholson finite difference method. In this chapter, we set up the numerics for each problem.

3.1 Bulk Potential

In Chapter II, a one-dimensional problem for the potential in the bulk is derived. For sake of argument, the time variable is suppressed in the following discussion. The resulting problem is

$$\kappa w_b \frac{\partial^2 E_b}{\partial x^2} = i(E_b), \tag{3.1}$$

$$\frac{\partial E_b}{\partial x}(0) = 0, \tag{3.2}$$

$$\frac{\partial E_b}{\partial x}(L_b) = 0. \tag{3.3}$$

The bvp4c solver in MATLAB requires input in a specific format. First, the governing equation must be converted into a first order system. To do so, let

$$y(1) = E_b, \tag{3.4}$$

$$y(2) = \frac{\partial E_b}{\partial x}. \tag{3.5}$$

This converts equation (3.1) into the system

$$dydx(1) = y(1), \tag{3.6}$$

$$dydx(2) = \frac{i(y(1))}{\kappa w_b}. \tag{3.7}$$

To get $dydx(2)$, we take equation (3.1) and solve for $\frac{\partial^2 E_b}{\partial x^2}$.

The boundary conditions also must be set up in a vector. In general, $yl(1)$ and $yl(2)$ are used for $E_b(0)$ and $\frac{\partial E_b}{\partial x}(0)$, respectively, and $yr(1)$ and $yr(2)$ are used for $E_b(L_b)$ and $\frac{\partial E_b}{\partial x}(L_b)$. The entries in the vector must be equal to zero, so generally, we move all nonzero terms to one side. For the bulk problem, we have Neumann conditions set equal to zero, so we use

$$\begin{bmatrix} yl(2) - 0 \\ yr(2) - 0 \end{bmatrix}. \tag{3.8}$$

Using this formulation, we can input the equation into the bvp4c solver as it requires. The implementation of this can be seen in Appendix **??**.

3.2 Oxygen Depletion

In order to solve the oxygen depletion problem numerically, we use the Crank-Nicholson method. We start with a uniform grid with time step dt and spatial step

dx. This gives us the discretized x axis and t axis

$$\begin{aligned} x_i &= (i-1)dx, \qquad i = 1, ..., imax, \\ t_n &= (n-1)dt, \qquad j = 1, ..., jmax. \end{aligned} \tag{3.9}$$

Note that $x_{imax} = L_{cr}$ and t_{nmax} is the amount of time we consider for the problem. The Crank-Nicholson method requires the problem to be discretized at $(x_i, t_{n+\frac{1}{2}})$. Denoting $u(x_i, t_n) = u_i^n$, the discretization of equation (2.34) and conditions (2.35)-(2.37) results in

$$\frac{u_i^{n+1} - u_i^n}{2(dt/2)} = D_O \frac{u_{i-1}^{n+\frac{1}{2}} - 2u_i^{n+\frac{1}{2}} + u_{i+1}^{n+\frac{1}{2}}}{dx^2} - \frac{i_O}{4w_{cr}F_a}\Big(\frac{u_i^{n+\frac{1}{2}}}{O_{2bulk}}\Big). \tag{3.10}$$

Because $t_{n+\frac{1}{2}}$ is not on the grid, the Crank-Nicholson method replaces each term evaluated at time $t_{n+\frac{1}{2}}$ with an average of the values at t_n and t_{n+1}. This gives

$$\frac{u_i^{n+1} - u_i^n}{dt} = \frac{D_O}{2dx^2}\left[u_{i-1}^{n+1} + u_{i-1}^n - 2(u_i^{n+1} + u_i^n) + u_{i+1}^{n+1} + u_{i+1}^n\right] - \frac{i_O}{8w_{cr}F_a}\Big(\frac{u_i^{n+1} + u_i^n}{O_{2bulk}}\Big). \tag{3.11}$$

If we group like u terms together to more easily see the weights of each point, we get

$$\begin{aligned} -\Big(\frac{\tilde{r}_O}{2}\Big)u_{i-1}^{n+1} + \Big(1 + \tilde{r}_O + \frac{i_O dt}{8w_{cr}F_a O_{2bulk}}\Big)u_i^{n+1} - \Big(\frac{\tilde{r}_O}{2}\Big)u_{i+1}^{n+1} = \\ \Big(\frac{\tilde{r}_O}{2}\Big)u_{i-1}^{n} + \Big(1 - \tilde{r}_O - \frac{i_O dt}{8w_{cr}F_a O_{2bulk}}\Big)u_i^{n} + \Big(\frac{\tilde{r}_O}{2}\Big)u_{i+1}^{n}, \end{aligned} \tag{3.12}$$

where $\tilde{r}_O = D_O dt/dx^2$. Discretizing the boundary conditions using the first order backwards difference on the Neumann condition, we get

$$\begin{aligned} u_1^n &= O_{2bulk}, \\ \frac{u_{imax}^n - u_{imax-1}^n}{dx} &= 0, \end{aligned} \tag{3.13}$$

which leads to

$$u_{imax}^n - u_{imax-1}^n = 0. \tag{3.14}$$

Discretizing the initial condition yields

$$u_i^1 = O_{2bulk}. \tag{3.15}$$

Using the discretized equation and conditions, we solve the following system of equations using a tridiagonal solver in MATLAB:

$$\begin{bmatrix} 1 & 0 & 0 & & ... \\ \text{gm} & 1+\text{gc} & \text{gp} & 0 & ... \\ 0 & \text{gm} & 1+\text{gc} & \text{gp} & ... \\ & \ddots & \ddots & \ddots & \\ ... & 0 & \text{gm} & 1+\text{gc} & \text{gp} \\ ... & 0 & 0 & -1 & 1 \end{bmatrix} \begin{bmatrix} u_1^{n+1} \\ u_2^{n+1} \\ ... \\ u_{imax-1}^{n+1} \\ u_{imax}^{n+1} \end{bmatrix} = \begin{bmatrix} O_{2bulk} \\ ... \\ \text{rhs}(i) \\ ... \\ 0 \end{bmatrix}, \tag{3.16}$$

with

$$\text{gm} = \text{gp} = -\frac{\tilde{r}_O}{2}, \tag{3.17}$$

$$\text{gc} = \tilde{r}_O + \frac{i_O dt}{8 w_{cr} F_a O_{2bulk}}, \tag{3.18}$$

$$\text{rhs}(i) = -(\text{gm})u_{i-1}^n + (1-\text{gc})u_i^n - (\text{gp})u_{i+1}^n. \tag{3.19}$$

3.3 Crevice Potential

We also solve the problem for the potential in the crevice using the bvp4c solver in MATLAB. The difference for the crevice problem is the boundary conditions. The conditions we use in the crevice are

$$E_{cr}(0) = E_{mouth}, \tag{3.20}$$

$$E_{cr}(L_{cr}) = E_{tip}. \tag{3.21}$$

The vector we use for these conditions is

$$\begin{bmatrix} yl(1) - E_{mouth} \\ yr(1) - E_{tip} \end{bmatrix}. \tag{3.22}$$

The details of the implementation of this are shown in Appendix **??**.

3.4 Aluminum Concentration

To solve the aluminum ion concentration problem, we discretize the problem using the same scheme as with the oxygen depletion problem. The only difference here is the source term. The discretized problem, taken from (2.51), is

$$\frac{C_i^{n+1} - C_i^n}{dt} = \frac{D_A}{2dx^2}\left[C_{i-1}^{n+1} + C_{i-1}^n - 2(C_i^{n+1} + C_i^n) + C_{i+1}^{n+1} + C_{i+1}^n\right] + \frac{i_A(x_i, t_n)}{Zw_{cr}F_a}. \tag{3.23}$$

Again, if we combine like C terms, we get

$$\begin{aligned} -\left(\frac{\tilde{r}_A}{2}\right)C_{i-1}^{n+1} + (1 + \tilde{r}_A)C_i^{n+1} - \left(\frac{\tilde{r}_A}{2}\right)C_{i+1}^{n+1} = \\ \left(\frac{\tilde{r}_A}{2}\right)C_{i-1}^n + (1 - \tilde{r}_A)C_i^n + \left(\frac{\tilde{r}_A}{2}\right)C_{i+1}^n + \frac{i_A(x_i, t_n)}{Zw_{cr}F_a}, \end{aligned} \tag{3.24}$$

where $\tilde{r}_A = \dfrac{D_A dt}{dx^2}$. Discretizing the boundary conditions using the first order backwards difference on the Neumann condition, we get

$$\begin{aligned} C_1^n &= Al_{bulk}, \\ \frac{C_{imax}^n - C_{imax-1}^n}{dx} &= 0, \end{aligned} \tag{3.25}$$

which leads to

$$C_{imax}^n - C_{imax-1}^n = 0. \tag{3.26}$$

The discretized initial condition is

$$C_i^1 = Al_{bulk}. \tag{3.27}$$

Using the discretized equation and conditions, we again solve the following system of equations using a tridiagonal solver in MATLAB:

$$\begin{bmatrix} 1 & 0 & 0 & 0 & ... \\ -\frac{\tilde{r}_A}{2} & 1+\tilde{r}_A & -\frac{\tilde{r}_A}{2} & 0 & ... \\ 0 & -\frac{\tilde{r}_A}{2} & 1+\tilde{r}_A & -\frac{\tilde{r}_A}{2} & ... \\ & \ddots & \ddots & \ddots & \\ ... & 0 & -\frac{\tilde{r}_A}{2} & 1+\tilde{r}_A & -\frac{\tilde{r}_A}{2} \\ ... & 0 & 0 & -1 & 1 \end{bmatrix} \begin{bmatrix} C_1^{n+1} \\ C_2^{n+1} \\ ... \\ C_{imax-1}^{n+1} \\ C_{imax}^{n+1} \end{bmatrix} = \begin{bmatrix} Al_{bulk} \\ ... \\ \text{rhs}(i) \\ ... \\ 0 \end{bmatrix}, \tag{3.28}$$

with $\text{rhs}(i) = \frac{\tilde{r}_A}{2}C_{i-1}^n + (1-\tilde{r}_A)C_i^n + \frac{\tilde{r}_A}{2}C_{i+1}^n + \frac{i_A(x_i,t_n)}{Zw_{cr}F_a}$. The code for this is shown in Appendix **??**.

CHAPTER IV

CONCLUSION

In this thesis, a fastener assembly is considered, with AA7075 as the plate and stainless steel as the fastener. A scheme is developed to model the initial stages of corrosion in both the bulk electrolyte and the crevice region formed between the fastener and the plate. The model combines aspects of galvanic, pitting, and crevice corrosion, which has not previously been done. Equations modeling the potential, oxygen concentration, and aluminum ion concentration in the crevice, as well as the potential in the bulk are developed. The problems in the bulk electrolyte and in the crevice are solved using the bvp4c boundary value problem solver in MATLAB, and the problems for the aluminum ion concentration and the oxygen concentration are solved numerically using the Crank-Nicholson method in MATLAB.

BIBLIOGRAPHY

[1] A. Stenta, S. Basco, A. Smith, C.B Clemons, D. Golovaty, K.L. Kreider, J. Wilder, G.W. Young, and R.S. Lillard. One-dimensional approach to modeling damage evolution in galvanic corrosion. *Corrosion Science*, 88:36–48, 2014.

[2] R.S. Lillard. Personal communication.

[3] A.M. Colwell. Developement of a stochastic metastable pit initiation model with transition to a stable pit state. Master's thesis, University of Akron, 2016.

[4] M.D. Brackman, C.B. Clemons, D. Golovaty, K.L. Kreider, J. Wilder, G.W. Young, J. Payer, and R.S. Lillard. Modeling and simulation of damage evolution during crevice corrosion. *Journal of the Electrochemical Society*, 161(5):C237–C245, 2014.

[5] K.B. Deshpande. Validated numerical modelling of galvanic corrosion for couples: Magnesium alloy (AE44)–mild steel and AE44– aluminium alloy (AA6063) in brine solution. *Corrosion Science*, 52(10):3514–3522, 2010.

[6] G.S. Frankel. Pitting corrosion of metals: A review of the critical factors. *Journal of the Electrochemical Society*, 145(6):2186–2198, 1998.

[7] N. Birbilis, M.K. Cavanaugh, and R.G. Buchheit. Electrochemical behavior and localized corrosion associated with Al_7Cu_2Fe particles in aluminum alloy 7075-T651. *Corrosion Science*, 48(12):4202–4215, 2006.

[8] M.K. Cavanaugh. *Modeling the environmental dependence of localized corrosion evolution in AA7075-T651.* PhD dissertation, The Ohio State University, 2009.

[9] J.R. Davis. *Corrosion of aluminum and aluminum alloys.* ASM International, 1999.

[10] E. McCafferty. Sequence of steps in the pitting of aluminum by chloride ions. *Corrosion Science*, 45(7):1421–1438, 2003.

[11] J.M. McKinnon. Corrosion damage evolution of a single pit. Master's thesis, University of Akron, 2015.

[12] E.G. Webb and R.C. Alkire. Pit initiation at single sulfide inclusions in stainless steel I. electrochemical microcell measurements. *Journal of the Electrochemical Society*, 149(6):B272–B279, 2002.

[13] M.G. Alvarez and J.R. Galvele. The mechanism of pitting of high purity iron in NaCl solutions. *Corrosion Science*, 24(1):27–48, 1984.

[14] S.B. De Wexler and J.R. Galvele. Anodic behavior of aluminum straining and a mechanism for pitting. *Journal of the Electrochemical Society*, 121(10):1271–1276, 1974.

[15] G.S. Frankel, L. Stockert, F. Hunkeler, and H. Boehni. Metastable pitting of stainless steel. *Corrosion*, 43(7):429–436, 1987.

[16] S.T. Pride, J.R. Scully, and J.L. Hudson. Metastable pitting of aluminum and criteria for the transition to stable pit growth. *Journal of the Electrochemical Society*, 141(11):3028–3040, 1994.

[17] J.R. Galvele. Transport processes and the mechanism of pitting of metals. *Journal of the Electrochemical Society*, 123(4):464–474, 1976.

[18] M.G. Alvarez, C. Manfredi, M. Giordano, and J.R. Galvele. Anodic rate-controlling steps in transgranular stress corrosion cracking of α-brass in nano$_2$ solutions. *Corrosion Science*, 24(9):769–780, 1984.

[19] P.S. Young. Modeling and analysis for atmospheric galvanic corrosion of fasteners in aluminum. Master's thesis, University of Akron, 2015.

[20] A. Stenta. *Species Dependent Modeling of Crevice Corrosion Systems.* PhD dissertation, University of Akron, 2015.

[21] G.F. Kennell, R.W. Evitts, and K.L. Heppner. A critical crevice solution and IR drop crevice corrosion model. *Corrosion Science*, 50(6):1716–1725, 2008.

[22] K. Hebert and R. Alkire. Dissolved metal species mechanism for initiation of crevice corrosion of aluminum II. mathematical model. *Journal of the Electrochemical Society*, 130(5):1007–1014, 1983.

[23] C. Liu, V.N. Rafla, J.R. Scully, and R.G. Kelly. Mathematical modeling of potential and current distributions for atmospheric corrosion of galvanic coupling in airframe components. In *CORROSION 2015*. NACE International, 2015.